2023 IEEE International Conference on Robotics and Automation (ICRA 2023)
May 29 - June 2, 2023. London, UK

A Force-Sensitive Exoskeleton for Teleoperation: An Application in Elderly Care Robotics

Alexander Toedtheide†, Xiao Chen, Hamid Sadeghian*, Abdeldjallil Naceri and Sami Haddadin

***Abstract*— With the increasing demand for new healthcare solutions and technologies, such as those resulting from the COVID-19 crisis, and the growing elderly population, exoskeletons for teleoperation are a promising solution for many future medical applications. In this context, we propose *two* force-sensitive upper-limb exoskeletons for teleoperation, that are characterized by: i) torque-controlled robotic actuators, ii) rigid-body model compensations, and iii) a lightweight design achieved through the use of Bowden cable transmissions and remotely placed actuators. Specifically, we present a *semi-active* upper-limb exoskeleton for which we demonstrate human-device interaction control and bilateral teleoperation with force-feedback, evaluated via simulation, in the lab and over the Internet. We also introduce a design for a future *fully-active* upper-limb exoskeleton with two contact force/torque sensors, for a dual-arm device, which features a novel 3-degrees-of-freedom exoskeleton shoulder design and a contact wrench mitigation controller, as demonstrated through simulation. With this work, we propose the essential technical steps towards a novel teleoperation system for elderly care.**

I. INTRODUCTION

With the elderly population steadily growing worldwide, there is a rising demand for home healthcare due to the shortage of healthcare workers (HCWs). A home healthcare robot, like GARMI [1], provides a potential solution for this shortage and flexibility to HCWs in terms of time and patient management. For instance, force-sensitive exoskeletons designed for robotic teleoperation with haptic feedback, allow HCWs to use GARMI as an avatar [2] for remote healthcare scenarios. This scenario does not only reduce the time and costs of patients and HCWs, but also reduces the exposure to infectious diseases, such as COVID-19 [3], [4]. Tele-healthcare provides access to safe, high-quality and essential healthcare services to people with mobility issues (e.g. people living in rural and remote areas, and elderly people) [5]. In particular, haptic interfaces allow the operators, and especially doctors, to send position commands and receive force-feedback from the patients' site in addition to the well-established audio-visual feedback. This is crucial for some examinations that require doctors' sense of touch, for instance, abdominal anomalies and breast cancer [4], [6], [7].

Therein, the exoskeleton of this work is proposed as a haptic input interface for the GARMI robot to e.g. remotely examine a patient using the world-wide infrastructure of the Internet, see Fig. 1.

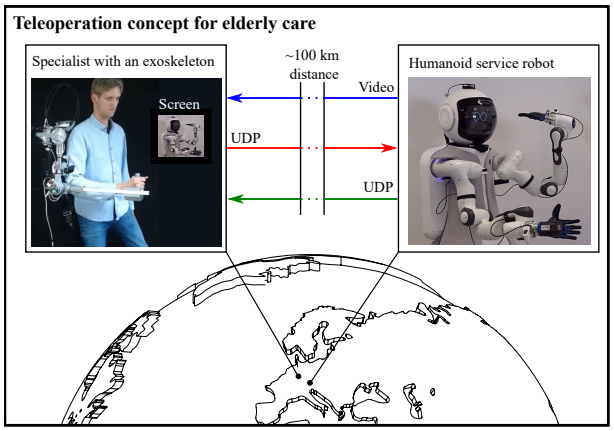

Fig. 1: Teleoperation of the GARMI robot via an exoskeleton

A. Literature Review

Current exoskeletons for teleoperation are able to map the human pose to the remote robot arm using the encoder of the joints [8], [9]. Alternatively, they can map the interaction forces from the remote robot system to the human [10], [11]. Some bi-manual-arm teleoperation systems also use the industrial robot on the leader side [12]. However, the moving inertia of such a system is high, and the force feedback can only be applied on the operator's hand, instead of the whole arm.

Many exoskeletons target rather simple designs and place the robotic joints directly at the joint axis [13]–[15]. Others increase the number of actuators for an improved workspace [16]. However, these design approaches tend to get bulky and heavy, since an additional motor mass needs be compensated by an even larger motor size. For tackling this problem, remote actuation via Bowden cables appears to be a promising solution, as this provides lightweight yet strong structures and high actuation dynamics [17]. Some interesting first designs have already been shown in [18]–[21], which still focus on rather low interaction forces, and which do not contain contact force measurement.

Exoskeletons require special sensor and control strategies, as discussed below. As the exoskeleton is directly attached to the human, the system should follow the motion of the operator, not vice versa. A key feature for achieving this behavior is the use of torque-controlled robot joints [19] [20], which allow for force sensitivity, back-drivability, and human-inspired impedance. Based on torque-controlled joints, impedance control [22] has been applied in several exoskeletons [19], [23]. The impedance controller shapes the

We gratefully acknowledge the funding of the Lighthouse Initiative Geriatronics by StMWi Bayern (Project X, grant no. IUK-1807-0007// IUK582/001) and LongLeif GaPa GmbH (Project Y). The authors acknowledge the financial support by the Federal Ministry of Education and Research of Germany (BMBF) in the programme of "Souverän. Digital. Vernetzt." Joint project 6G-life, project identification number 16KISK002. Please note that S. Haddadin has a potential conflict of interest as shareholder of Franka Emika GmbH.

All authors are with Chair of Robotics and Systems Intelligence, Munich School of Robotics and Machine Intelligence, Technical University of Munich, 80797 Munich, Germany *and Faculty of Engineering, University of Isfahan, 8174673441 Isfahan, Iran. †Corresponding Author alexander.toedtheide@tum.de

relation between exoskeleton end-effector position and the joint torque. Another possibility to realize the guidance of a human operator via interaction forces is admittance control, which shapes the relationship between exoskeleton force and joint position. Admittance control allows the exoskeleton to appear much lighter by controlling the interaction force, which is measured by Force/Torque (F/T)-sensor in contact with the human body. Some designs use multi-axis F/T-sensors at the exoskeleton end-effector to estimate the wrench applied by the human [15], [24].

Exoskeletons for teleoperation are applied in tasks from different areas. Manipulation tasks in the industry like turning switches in ISS mockup [11], connecting 380V plugs [25] and stiffness distinction [26] are realized by using an exoskeleton to teleoperate a humanoid robot or robot arms. In the medical area, the exoskeleton ARMin is used in tele-rehabilitation, where the motion can be learned by the remote side, and the operator can feel if the remote side is actively participating in the rehabilitation [27]. Typical real-world tasks in teleoperation, that improve the quality of life of the elderly, when performed by a robot, include lifting boxes [11], [25] or opening a door [28]. Table I compares the properties between our design and other exoskeletons that are used for teleoperation.

	Limb inertia	**Portable**	**Haptic tele feedback**	**Force contact control**	**Remote actuation**
Ours	+	✓	✓	(✓)*	Yes
TABLIS [29]	−	×	✓	×	No
ARMin IV [30]	−	×	✓	✓	No
SAM [31]	−	✓	✓	×	No
ALEx [32]	−	×	✓	×	Yes
exoskeleton [33]	+	✓	×	×	Passive
Capio [11]	−	✓	✓	×	No
exoskeleton [34]	+	×	✓	×	Yes

TABLE I: Comparison of exoskeletons used for teleoperation. High/low limb inertia is -/+ from estimate. *Proof of concept in simulation and CAD.

B. Motivation

A teleoperation system combines human intelligence with the remote robot's physical body. This has several advantages. Firstly, it enables the robot to execute tasks that are currently difficult for robots, such as medical examination. Secondly, the system allows HCWs to provide remote assistance to the elderly and patients without being physically present.

For current active exoskeletons, electromechanical actuators are the main source of actuation because of their supreme control characteristics. The actuators are often placed next to the robot joints which however i) increase the limb inertia, ii) require more energy for acceleration, iii) reduce robot safety and iv) also reduce the transparency of the whole mechanism. This is specifically crucial for an exoskeleton which is attached to the human. Reshaping of this inertia through a torque controlled interface demands extra effort by embedded force torque sensing relying on high-speed control loop [35]. However, a more wise solution is to relocate the actuators as much as possible from the stationary base of the robot to the backpack.

In this work, a lightweight exoskeleton is proposed, and applied for tele-healthcare scenarios. Specifically, we propose two exoskeletons (i.e. semi-active and fully-active) including control and teleoperation architecture which are used for operating a remotely controlled GARMI robot. The systems are actuated by Bowden cables to allow designing lower weight and inertia structures by placing the actuators at a remote location. Custom-made robot joints with a specially designed torque sensor are implemented to provide a seamless, backdrivable, torque-controlled, and strong actuator. This hardware concept is the foundation of the control strategy: The controller is designed in such a way that the exoskeleton follows the attached human arm only via interaction forces and real-time models reduce the mechanical properties of the system such as gravity influences.

The contributions of this work are:

- A technical realization of a teleoperation concept for elderly care, see Fig. 1, which includes i) an exoskeleton-based haptic control device and ii) a tactile service robot, whereas both interact via bilateral force-sensitive control.
- Two single-sided lightweight 4-degrees-of-freedom (dof) upper-limb exoskeleton designs for teleoperation:
  - A *semi-active* exoskeleton[1], featuring a $\underline{RRRR}$ kinematics, which is realized in hardware and examined by experiments.
  - A *fully-active* exoskeleton[2], featuring a $\underline{RRRR}$ kinematics and two FT sensors in the contact points between human and device, for which a computer-aided design (CAD) is provided.
- A force-sensitive control concept for the proposed human-robot-exoskeleton teleoperation system, with optional wrench mitigating controller (using the FT-sensors), which is investigated by a rigid-body controller simulation for the cases of i) human-interaction control and i) bilateral teleoperation.
- An experimental evaluation of the human-exoskeleton interaction as well as human-exoskeleton teleoperation within the lab and over the Internet (100 km distance).

The remainder of this paper is structured as follows. Section II and Sec. III deal with the modeling and control of the proposed systems. Section IV presents the mechanical design of the exoskeletons. Section V shows the simulation study of the human-exoskeleton interaction, as well as a simulation of force-feedback teleoperation. Section VI discusses the validation of the teleoperation capabilities of the systems via several experiments. Section VII concludes the paper.

II. Modeling

The teleoperation system is modeled by three separate serial kinematics, namely an exoskeleton (E), a human (H) and a robot (R), depicted in Fig. 2. These systems are described in generalized coordinates $\boldsymbol{q}_{\mathrm{E}} \in \mathbb{R}^{m_{\mathrm{E}}\times 1}$, $\boldsymbol{q}_{\mathrm{H}} \in \mathbb{R}^{m_{\mathrm{H}}\times 1}$ and $\boldsymbol{q}_{\mathrm{R}} \in \mathbb{R}^{m_{\mathrm{R}}\times 1}$ with $m_{\mathrm{E}} = 4$, $m_{\mathrm{H}} = 7$ and $m_{\mathrm{R}} = 7$.

[1]The RRR shoulder of this exoskeleton is based on our wearable shoulder exoskeleton prototype from [36].

[2]A bimanual design, required to operate both arms of the GARMI robot in the future, is proposed, as well.

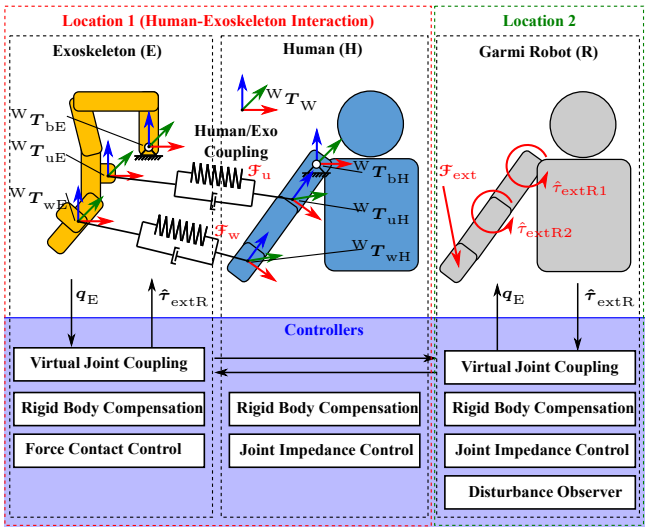

Fig. 2: Systems and controllers of the robot teleoperation

Based on the system kinematics[3], the dynamics of each system follows as

$$\boldsymbol{M}_{\mathrm{E}}(\boldsymbol{q}_{\mathrm{E}})\ddot{\boldsymbol{q}}_{\mathrm{E}} + \boldsymbol{C}_{\mathrm{E}}(\boldsymbol{q}_{\mathrm{E}}, \dot{\boldsymbol{q}}_{\mathrm{E}})\dot{\boldsymbol{q}}_{\mathrm{E}} + \boldsymbol{g}_{\mathrm{E}}(\boldsymbol{q}_{\mathrm{E}}) = \boldsymbol{\tau}_{\mathrm{E}} + \boldsymbol{\tau}_{\mathrm{extE}} \tag{1}$$

$$\boldsymbol{M}_{\mathrm{H}}(\boldsymbol{q}_{\mathrm{H}})\ddot{\boldsymbol{q}}_{\mathrm{H}} + \boldsymbol{C}_{\mathrm{H}}(\boldsymbol{q}_{\mathrm{H}}, \dot{\boldsymbol{q}}_{\mathrm{H}})\dot{\boldsymbol{q}}_{\mathrm{H}} + \boldsymbol{g}_{\mathrm{H}}(\boldsymbol{q}_{\mathrm{H}}) = \boldsymbol{\tau}_{\mathrm{H}} + \boldsymbol{\tau}_{\mathrm{extH}} \tag{2}$$

$$\boldsymbol{M}_{\mathrm{R}}(\boldsymbol{q}_{\mathrm{R}})\ddot{\boldsymbol{q}}_{\mathrm{R}} + \boldsymbol{C}_{\mathrm{R}}(\boldsymbol{q}_{\mathrm{R}}, \dot{\boldsymbol{q}}_{\mathrm{R}})\dot{\boldsymbol{q}}_{\mathrm{R}} + \boldsymbol{g}_{\mathrm{R}}(\boldsymbol{q}_{\mathrm{R}}) = \boldsymbol{\tau}_{\mathrm{R}} + \boldsymbol{\tau}_{\mathrm{extR}}, \tag{3}$$

where $\boldsymbol{M}(\boldsymbol{q}) \in \mathbb{R}^{m\times m}$ is the inertia matrix, $\boldsymbol{C}(\boldsymbol{q}, \dot{\boldsymbol{q}}) \in \mathbb{R}^{m\times m}$ is Coriolis/centrifugal matrix, and $\boldsymbol{g}(\boldsymbol{q}) \in \mathbb{R}^{m\times 1}$ is the gravity vector, $\boldsymbol{\tau} \in \mathbb{R}^{m\times 1}$ is the joint torque and $\boldsymbol{\tau}_{\mathrm{ext}} \in \mathbb{R}^{m\times 1}$ the vector of external torques, omitting the indices for simplicity. Note that the dynamic of the human is assumed to be given by a geometric and density assumptions. This enables us to give a detailed human-robot interaction analysis. Exoskeleton and human are coupled via

$$\begin{pmatrix} \boldsymbol{\tau}_{\mathrm{extE}} \\ \boldsymbol{\tau}_{\mathrm{extH}} \end{pmatrix} = \begin{pmatrix} \boldsymbol{J}_{\mathrm{uE}}(\boldsymbol{q}_{\mathrm{E}})^T & \boldsymbol{J}_{\mathrm{wE}}(\boldsymbol{q}_{\mathrm{E}})^T \\ -\boldsymbol{J}_{\mathrm{uH}}(\boldsymbol{q}_{\mathrm{H}})^T & -\boldsymbol{J}_{\mathrm{wH}}(\boldsymbol{q}_{\mathrm{H}})^T \end{pmatrix} \begin{pmatrix} {}^{W}\boldsymbol{\mathcal{F}}_{\mathrm{u}} \\ {}^{W}\boldsymbol{\mathcal{F}}_{\mathrm{w}} \end{pmatrix} \tag{4}$$

with $\boldsymbol{J}_{\mathrm{uE}}(\boldsymbol{q}_{\mathrm{E}})$, $\boldsymbol{J}_{\mathrm{wE}}(\boldsymbol{q}_{\mathrm{E}})$, $\boldsymbol{J}_{\mathrm{uH}}(\boldsymbol{q}_{\mathrm{H}})$, $\boldsymbol{J}_{\mathrm{wH}}(\boldsymbol{q}_{\mathrm{H}}) \in \mathbb{R}^{6\times m}$ being the Jacobians which are derived from the coordinate frames of the upper arm attachment ${}^{\mathrm{W}}\boldsymbol{T}_{\mathrm{uE}}$, ${}^{\mathrm{W}}\boldsymbol{T}_{\mathrm{uH}} \in \mathbb{R}^{4\times 4}$ and wrist attachment ${}^{\mathrm{W}}\boldsymbol{T}_{\mathrm{wE}}$, ${}^{\mathrm{W}}\boldsymbol{T}_{\mathrm{wH}} \in \mathbb{R}^{4\times 4}$, see Fig. 2, on human and exoskeleton side, respectively. ${}^{W}\boldsymbol{\mathcal{F}}_{\mathrm{u}} \in \mathbb{R}^{6\times 1}$ and ${}^{W}\boldsymbol{\mathcal{F}}_{\mathrm{w}} \in \mathbb{R}^{6\times 1}$ are the wrenches which occur between exoskeleton and human at upper arm (u) and wrist (w), with $\boldsymbol{\mathcal{F}} = (\boldsymbol{f}^T, \boldsymbol{m}^T)^T$, where $\boldsymbol{f} \in \mathbb{R}^{3\times 1}$ and $\boldsymbol{m} \in \mathbb{R}^{3\times 1}$ are the force and moment, respectively. For simplicity, $\boldsymbol{m} = \boldsymbol{0}$. These are modeled based on spring-damper systems as described in [36], utilizing the translational components (and its time derivatives), between ${}^{\mathrm{W}}\boldsymbol{T}_{\mathrm{uE}}$ and ${}^{\mathrm{W}}\boldsymbol{T}_{\mathrm{uH}}$, as well as ${}^{\mathrm{W}}\boldsymbol{T}_{\mathrm{wE}}$ and ${}^{\mathrm{W}}\boldsymbol{T}_{\mathrm{wH}}$. Consequently, the wrenches can be written as ${}^{W}\boldsymbol{\mathcal{F}}_{\mathrm{u}} := {}^{W}\boldsymbol{\mathcal{F}}_{\mathrm{u}}({}^{\mathrm{W}}\boldsymbol{T}_{\mathrm{uE}}, {}^{\mathrm{W}}\boldsymbol{T}_{\mathrm{uH}})$ and ${}^{W}\boldsymbol{\mathcal{F}}_{\mathrm{w}} := {}^{W}\boldsymbol{\mathcal{F}}_{\mathrm{w}}({}^{\mathrm{W}}\boldsymbol{T}_{\mathrm{wE}}, {}^{\mathrm{W}}\boldsymbol{T}_{\mathrm{wH}})$. All frames are described in world coordinates (w), requiring to map body related coordinate frames (E) and (H), via the base frame location ${}^{\mathrm{W}}\boldsymbol{T}_{\mathrm{bE}}$ and ${}^{\mathrm{W}}\boldsymbol{T}_{\mathrm{bH}}$, to the world frame (w), respectively.

[3]The kinematics of system (R) is essentially a Panda robot by Franka Emika GmbH, Germany [37]. The kinematics of systems (E) and (H) can be derived using modified DH-parameters from Fig. 3

III. Control

The controllers of exoskeleton (E), human (H) and robot (R) are

$$\boldsymbol{\tau}_{\mathrm{dE}} = \boldsymbol{\tau}_{\mathrm{ffE}} + \boldsymbol{\tau}_{\mathrm{vc}} + \hat{\boldsymbol{\tau}}_{\mathrm{E}} \tag{5}$$

$$\boldsymbol{\tau}_{\mathrm{dH}} = \boldsymbol{K}_{\mathrm{impH}}\boldsymbol{e}_{\mathrm{H}} + \boldsymbol{D}_{\mathrm{impH}}\dot{\boldsymbol{e}}_{\mathrm{H}} + \hat{\boldsymbol{\tau}}_{\mathrm{H}} \tag{6}$$

$$\boldsymbol{\tau}_{\mathrm{dR}} = \boldsymbol{K}_{\mathrm{impR}}\boldsymbol{e}_{\mathrm{R}} + \boldsymbol{D}_{\mathrm{impH}}\dot{\boldsymbol{e}}_{\mathrm{R}} + \hat{\boldsymbol{\tau}}_{\mathrm{R}}, \tag{7}$$

where human and robot are equipped with a joint impedance controller, where $\boldsymbol{K}_{\mathrm{imp}} \in \mathbb{R}^{m\times m}$ and $\boldsymbol{D}_{\mathrm{imp}} \in \mathbb{R}^{m\times m}$ are the joint stiffness and damping. $\boldsymbol{e} \in \mathbb{R}^{m\times 1}$ is the joint control error and $\boldsymbol{\tau}_{\mathrm{d}} \in \mathbb{R}^{m\times 1}$ is the desired joint torque controller input[4]. All three systems are equipped with a rigid body compensation $\hat{\boldsymbol{\tau}}_{\mathrm{E}}$, $\hat{\boldsymbol{\tau}}_{\mathrm{H}}$ and $\hat{\boldsymbol{\tau}}_{\mathrm{R}} \in \mathbb{R}^{m\times 1}$ which result from (1), (2) and (3), neglecting acceleration. A desired human joint motion is given by $\boldsymbol{q}_{\mathrm{dH}}$ and $\boldsymbol{e}_{\mathrm{H}} = \boldsymbol{q}_{\mathrm{dH}} - \boldsymbol{q}_{\mathrm{H}}$.

The feedforward term for the *force contact controller* is given by,

$$\boldsymbol{\tau}_{\mathrm{ffE}} = k_1 \left[\boldsymbol{J}_{\mathrm{uE}}(\boldsymbol{q}_{\mathrm{E}})^{T\,W}\boldsymbol{\mathcal{F}}_{\mathrm{u}} + \boldsymbol{J}_{\mathrm{wE}}(\boldsymbol{q}_{\mathrm{E}})^{T\,W}\boldsymbol{\mathcal{F}}_{\mathrm{w}}\right], \tag{8}$$

whereas $k_1 = \{0, 1\}$ is a binary key. The idea is to apply virtual contact wrenches ${}^{W}\hat{\boldsymbol{\mathcal{F}}}_{\mathrm{u}}$ and ${}^{W}\hat{\boldsymbol{\mathcal{F}}}_{\mathrm{w}}$ which act in addition to the physical ones[5] onto the system.

The *virtual joint coupling* between the robot's desired joint position and the exoskeleton joints is obtained by a joint position based coupling

$$\boldsymbol{e}_{\mathrm{R}} = \underbrace{\boldsymbol{P}\left(\boldsymbol{q}_{\mathrm{E}} - \boldsymbol{q}_{\mathrm{E},0}\right) + \boldsymbol{q}_{\mathrm{R},0}}_{\boldsymbol{q}_{\mathrm{dR}}} - \boldsymbol{q}_{\mathrm{R}}, \tag{9}$$

whereas the joint assignment between robot and exoskeleton is done by the sparse binary matrix $\boldsymbol{P}$, and the joint coordinate mapping by $\boldsymbol{q}_{\mathrm{E},0}$ and $\boldsymbol{q}_{\mathrm{R},0}$ for exoskeleton and robot, respectively. $\boldsymbol{q}_{\mathrm{dR}}$ corresponds to the desired joint position. Force feedback from the robot to the exoskeleton is realized by

$$\boldsymbol{\tau}_{\mathrm{vc}} = k_2 \boldsymbol{P}^T \hat{\boldsymbol{\tau}}_{\mathrm{extR}}, \tag{10}$$

with $k_2 = \{0, 1\}$ being a binary key. External joint torques of the robot $\hat{\boldsymbol{\tau}}_{\mathrm{extR}}$ are estimated by a generalized momentum observer [38].

IV. Mechanical Design

The mechatronics concept of each exoskeleton is based on physical human robot interaction (pHRI) [39], enabling a guidance of the system solely via interaction forces. For this, joint-torque-controlled actuators in combination with real-time-capable rigid body model compensations and controllers from Sec. III are used. Both systems utilize a light-weight exoskeleton kinematics which was designed for reducing the weight and inertia of all movable parts. This is enabled by i) light-weight aluminum structure elements,

[4]We assume ideal joint torque controllers via $\boldsymbol{\tau}_{\mathrm{d}} = \boldsymbol{\tau}$.

[5]In plant simulation, ${}^{W}\boldsymbol{\mathcal{F}}_{\mathrm{u}}$ and ${}^{W}\boldsymbol{\mathcal{F}}_{\mathrm{w}}$ are measured by the spring-damper systems, as described in [36]. In a future real system, ${}^{W}\boldsymbol{\mathcal{F}}_{\mathrm{u}}$ and ${}^{W}\boldsymbol{\mathcal{F}}_{\mathrm{w}}$ will be measured by a 6-dof force/torque sensor at (u) and (w), respectively.

ii) a remote actuator placement and iii) spool/Bowden-cable-transmissions between actuators and exoskeleton joints. Table II compares the features of the proposed systems of this work in contrast to our previous work [36] as well as the used investigation methods for the particular systems.

	Our work [36]	This work	
Name	ExoPro Gen I	SemiActiveTeleop	FullyActiveTeleop
Status	Realized	Realized, Fig. 3a	CAD, Fig. 3b,4
Application	Arm prosthetics	Teleoperation	Teleoperation
Wearable	Yes	Attached mode	Attached mode
Investigation	Sim + Exp	Exp, Fig. 8,9,10	Sim, Fig. 5,6
Shoulder	$\underline{RRR}$	$\underline{RRR}$	$\underline{RRR}$
Elbow	None	$\underline{R}$	$\underline{R}$
Contact sensing	None	None	2x 6 dof F/T
Dual Arm	No	No	Yes

TABLE II: Features and evolution of our exoskeletons.

1) Design I: Semi-active (single-arm) exoskeleton: The exoskeleton is based on a RRR gimbal-like shoulder kinematics design, mimicking the complex shoulder kinematics of the human, as well as on a single R joint following the motion of the human elbow joint, see Fig. 3a. While joint 1 was designed passive, joint 2 and 3 are actuated by Bowden cables (omitted in the image), using the spools to drive the exoskeleton elements. All three active joints of the exoskeleton are driven by the same-type, custom-made, torque-controlled robotic actuators. More information regarding the design and the hardware characteristics of the shoulder exoskeleton may be found in our work [36].

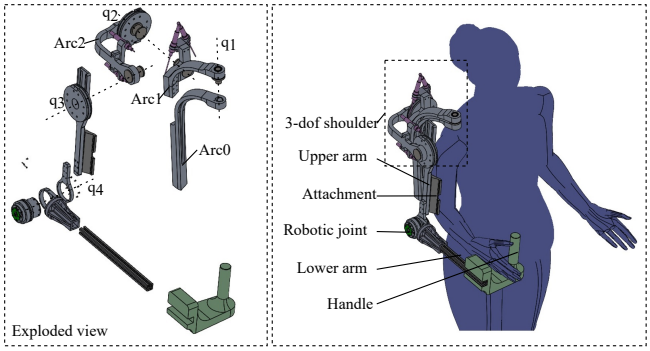

(a) Semi active single-sided shoulder exoskeleton (realized), Fig. 8

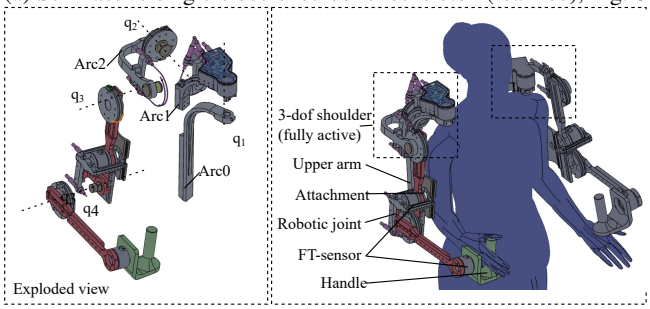

(b) Fully active dual-arm shoulder exoskeleton (design only)

Fig. 3: Upper limb exoskeletons of this work (simulated)

2) Design II: Fully-active (dual-arm) exoskeleton: The design of the fully-active exoskeleton is depicted in Fig. 3b. The system features four active dof and is also equipped with two 6-dof FT-sensors located at the hand and upper arm attachment between user and device. These FT-sensors allow for an implementation of a *force contact controller*, such as (8), mitigating the interaction forces between user and device and improving the back-drivability, and thus usability, of the system. The image also shows the potential of a dual-arm version of the exoskeleton.

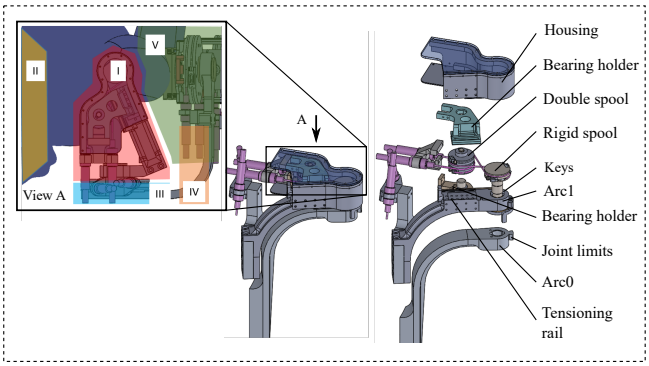

(a) Space requirements and exploded view of joint 1

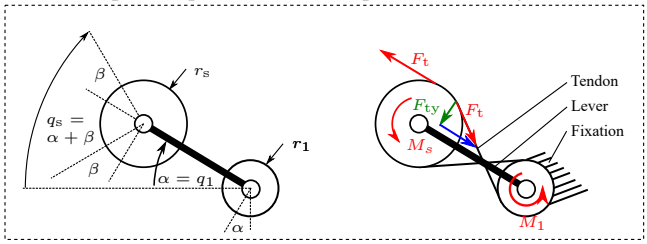

(b) Schematics

Fig. 4: Active shoulder rotation of joint 1

In the following, the new active shoulder rotation of the exoskeleton is proposed, see Fig 4a, and aims for providing a space-saving Bowden-cable-driven actuation concept for q_1 of the kinematics from Fig. 3a. Due to the truncated structure of the shoulder kinematics, the Bowden-cabled-based actuation solutions from q_2 and q_3 cannot be transferred to q_1. Instead, a new actuation concept is proposed, see Fig. 4a: The key idea is to fix the *rigid spool* to *Arc0* and twist *Arc1* around it, instead of rotating the spool directly (as in q_2 and q_3). This, however, requires the tendons to be i) in a cross arrangement and ii) to be nonparallel to the *lever*, since a non-negative tendon force component F_{ty} is required for a generation of the joint torque M_1, see Fig. 4b. A *double spool* is used in the joint design to control the angle of the leaving Bowden cables[6].

In the following, the kinematics of the joint is derived. Looking at Fig. 4b, the deflection of spool 1 and spool s can be described via α and β, respectively. The radii of spool 1 and s are r_1 and r_s. As spool 1 and s are connected via tendons in cross arrangement, it yields

$$\alpha r_1 = \beta r_s. \tag{11}$$

For the relation between q_1 and q_s it follows, with $q_1 = \alpha$,

$$q_s = \alpha + \beta \tag{12}$$

$$q_s = q_1 \left(1 + \frac{r_1}{r_s}\right). \tag{13}$$

[6]Otherwise, the Bowden cables would follow the orientation of the tendons in the cross arrangement, which results in a space-wasting Bowden cable routing.

The kinematic and mechanical relation can be derived based on the virtual work. It yields

$$\delta q_1 M_1 - \delta q_s M_\mathrm{s} = 0 \tag{14}$$

$$M_1 = \left(1 + \frac{r_1}{r_\mathrm{s}}\right) M_\mathrm{s} = \left(1 + \frac{r_1}{r_\mathrm{s}}\right) \frac{F_\mathrm{t}}{r_\mathrm{s}} \tag{15}$$

$$M_1 = i_\mathrm{g} M_\mathrm{s} \tag{16}$$

$$M_1 = 2\frac{F_\mathrm{t}}{r_\mathrm{s}}, \text{ for } r_1 = r_\mathrm{s} \tag{17}$$

where M_s is the torque affected by the Bowden cables, M_1 is the toque of the lever or the robotic joint and i_g is the corresponding gear ratio constant.

V. Simulation

Rigid body simulations were performed in Matlab/Simulink with a variable step solver to investigate the modeling and control concepts of this work. For a better understanding, the human-exoskeleton interaction of the simulation is depicted in Fig. 5. Here, the 7-dof model of the human (grey) is connected to a 4 dof exoskeleton (color) via the two attachment points at arm (u) and hand/wrist (w).

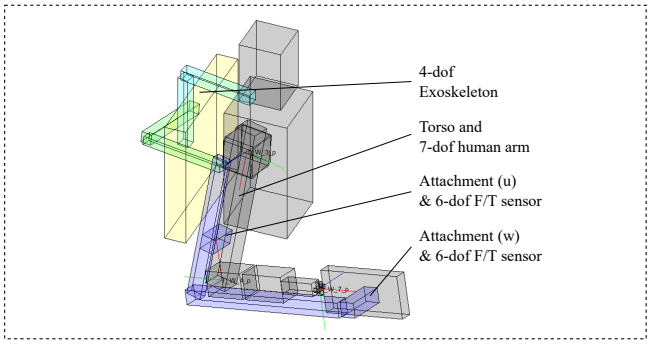

Fig. 5: Animation of the simulated exoskeleton with human attachment

The first simulation investigates the human-exoskeleton interaction at location 1, according to Fig. 2, and compares the interaction forces at (u) and (w) with/without *force contact control*. The first row of Fig. 6 depicts a sinusoidal joint motion using the human controller (6). It can be noticed that the joints of exoskeleton and human are seamlessly connected due to the coupling of these two systems via (4). The second and third row of Fig. 6 also show the actively mitigated interaction forces, when using the 6-dof F/T sensors and the *force contact controller* (8).

The second simulations investigate the teleoperation and force-feedback capabilities of the system. For this, the systems are coupled via (7), (9), (10) and considered to be at two different location 1 and 2, according to Fig. 2. The first row of Fig. 7 depicts the interaction force $\boldsymbol{F}_\mathrm{extR}$ which acts on the robot end effector via $\boldsymbol{\tau}_\mathrm{extR} = \boldsymbol{J}(\mathrm{EE}, \boldsymbol{q}_\mathrm{R})^T \boldsymbol{F}_\mathrm{extR}$ with $\boldsymbol{J}(\mathrm{EE}, \boldsymbol{q}_\mathrm{R})$ being the end effector Jacobian matrix. The second row shows the coupled motion of the robot and exoskeleton affected by $\boldsymbol{F}_\mathrm{extR}$. Note that the remaining control error between $\boldsymbol{q}_\mathrm{R}$ and $\boldsymbol{q}_\mathrm{E}$ is affected by damping response of the robot (R) which not fed back to the exoskeleton, see (10).

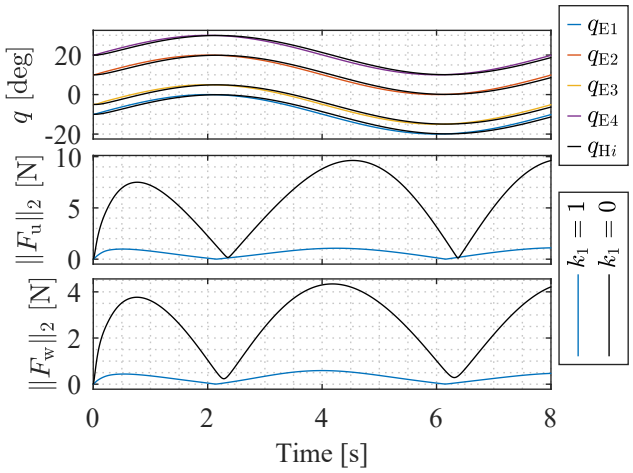

Fig. 6: Simulation: human-guided joint motion with/without *force contact controller*. Result: Interaction forces are mitigated.

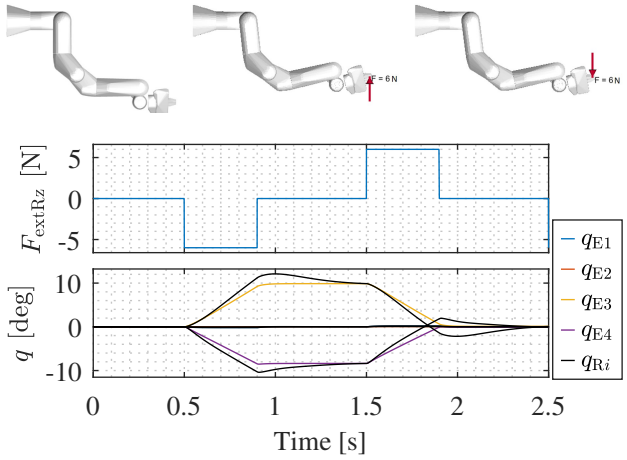

Fig. 7: Simulation: motion of the systems when applying a contact force at the remotely located robot

VI. Experiments

In this section, the single-sided exoskeleton is validated in tele-manipulation using the GARMI robot [1]. The exoskeleton runs with a Matlab/Simulink on a Linux machine with a real-time kernel. The GARMI robot is also controlled in real-time through a dedicated ROS architecture. The exoskeleton and the robot are connected via the Unified Datagram Protocol (UDP), transferring joint positions and velocities of the exoskeleton, and external torques of the robot at 1 kHz. As the kinematics of robot and exoskeleton complement each other, a joint-to-joint mapping of angles and torques is performed by (9). By this, the motion of the exoskeleton is mirrored to the robot.

For the first experiment, the robot and exoskeleton are connected to the same network (delay of less than 1 ms) and are placed at the same location. The exoskeleton is used to teleoperate the right arm of GARMI considering the two cases i) without force feedback, see Fig. 8 ($k_2 = 0$), and ii)

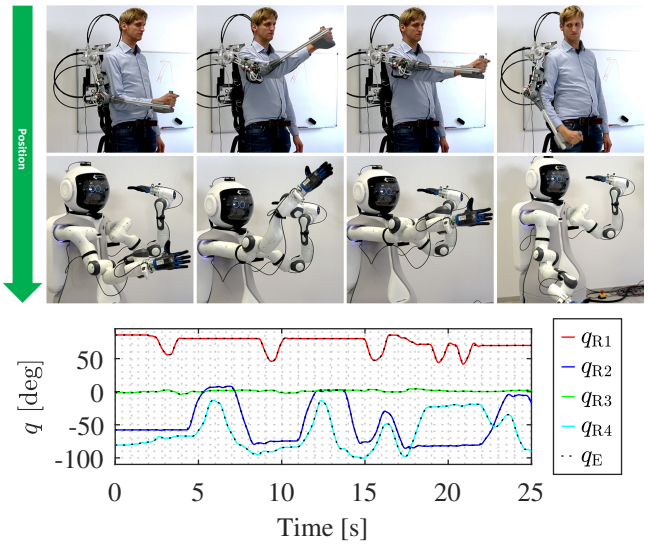

Fig. 8: Exoskeleton angular tracking in the same lab

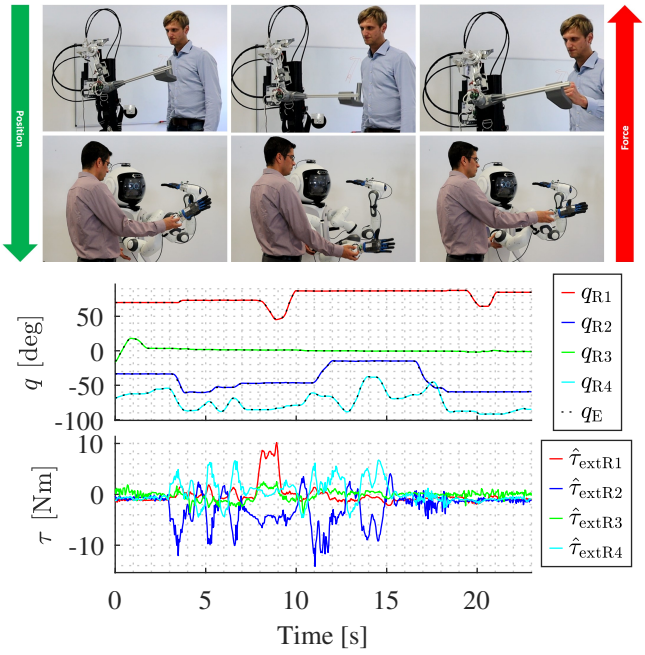

Fig. 9: Exoskeleton in interaction in the same lab

with bi-directional communication via the force feedback, see Fig. 9 ($k_2 = 1$). Note that the joint angles of the exoskeleton and the robot are shown in the same figure. The second operator on the robot side can move the exoskeleton freely, due to the applied torque control schemes given by (10), while the interaction on the teleoperated robot arm can be felt with accepted level of transparency, see Fig. 9.

In the next experiment, the performance of the teleoperated system over a large distance is illustrated. For the sake of simplicity, one arm of the robot is utilized for this teleoperation experiment. The exoskeleton is located in the Laboratory in Munich and the robot is located at the Geriatronic center in Garmisch-Partenkirchen which are approximately 100km away from each other. Additionally,

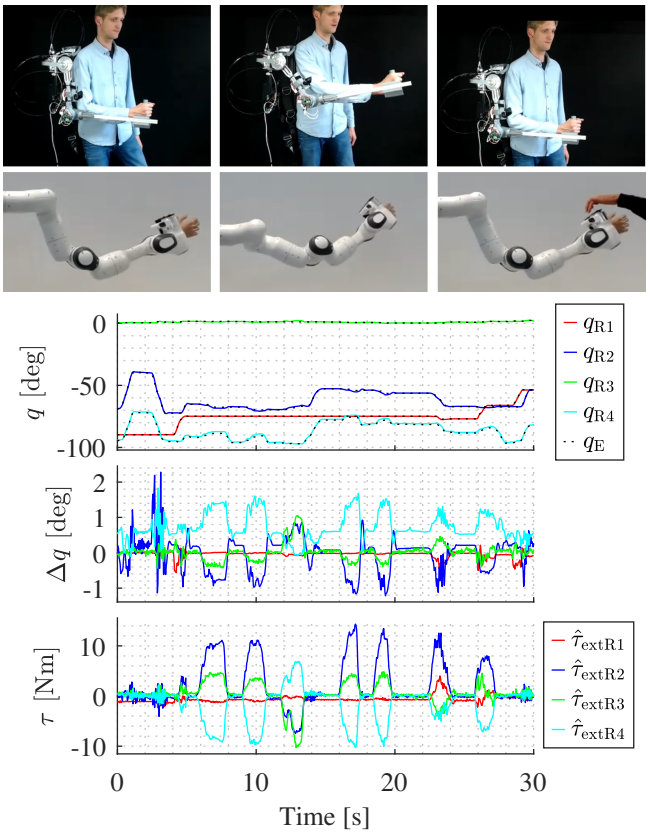

Fig. 10: Exoskeleton tracking and interaction over 100 km distance

the operator of the exoskeleton receives live video data of the robot via a video conference software to obtain visual feedback. The experiment, comprising the exoskeleton-based teleoperation over the internet, is illustrated in Fig. 10. The joint tracking performance, the control error, as well as the interaction torques during this bilateral teleoperation are depicted in the figure. It can be seen that the exoskeleton and the robot follow each other perfectly, while the systems are in physical interaction with the other one, respectively. The video of the above simulations and experiments are provided in the multi media attachment of this paper.

VII. CONCLUSION

This paper proposed two designs of lightweight exoskeletons that can be used as force-sensitive haptic interfaces for controlling remotely located robot arms. Specifically, the systems were designed for teleoperation of the Garmi robot in daily-life tasks. A semi-active exoskeleton with 4-dof (3-dof-actuated) was introduced and its performance for interaction control and tele-manipulation was investigated through simulation study as well as several experiments. The results illustrate that the system can be used effectively for transparent tele-manipulation even over 100 km of distance. Based on the first single-sided prototype design, a fully-active (4-dof-actuated) exoskeleton is further introduced towards bi-manual teleoperation. Further research will concentrate on realizing the bimanual-arm system and the experimental implementation of the force feedback control.

REFERENCES

[1] M. Tröbinger, C. Jähne, Z. Qu, J. Elsner, A. Reindl, S. Getz, T. Goll, B. Loinger, T. Loibl, C. Kugler *et al.*, "Introducing garmi-a service robotics platform to support the elderly at home: Design philosophy, system overview and first results," *IEEE Robotics and Automation Letters*, vol. 6, no. 3, pp. 5857–5864, 2021.

[2] S. Haddadin, L. Johannsmeier, and F. Díaz Ledezma, "Tactile robots as a central embodiment of the tactile internet," *Proceedings of the IEEE*, vol. 107, no. 2, pp. 471–487, 2019.

[3] A. Smith, E. Thomas *et al.*, "Telehealth for global emergencies: Implications for coronavirus disease 2019 (covid-19)," *Journal of Telemedicine and Telecare*, vol. 26, no. 5, pp. 309–313, 2020, cited By 241.

[4] A. Naceri, J. Elsner, M. Tröbinger, H. Sadeghian, L. Johannsmeier, F. Voigt, X. Chen, D. Macari, C. Jähne, M. Berlet, J. Fuchtmann, L. Figueredo, H. Feußner, D. Wilhelm, and S. Haddadin, "Tactile robotic telemedicine for safe remote diagnostics in times of corona: System design, feasibility and usability study," *IEEE Robotics and Automation Letters*, vol. 7, no. 4, pp. 10 296–10 303, 2022.

[5] G. Palozzi, I. Schettini, and A. Chirico, "Enhancing the sustainable goal of access to healthcare: Findings from a literature review on telemedicine employment in rural areas," *Sustainability*, vol. 12, no. 8, 2020. [Online]. Available: https://www.mdpi.com/2071-1050/12/8/3318

[6] Y. Shen, C. Pomeroy, N. Xi, N. Methil-Sudhakaran, R. Mukherjee, D. Zhu, M. Mutka, C. Slomski, and K. Apelgren, "Supermedia interface for internet based tele-diagnostics of breast pathology," in *IEEE/RAS-EMBS International Conference on Biomedical Robotics and Biomechatronics*, 2006, pp. 787–792.

[7] Y. Shen, N. Xi, N. Methil-Sudhakaran, R. Mukherjee, D. Zhu, Z. Cen, M. W. Mutka, C. A. Slomski, and K. N. Apelgren, "Internet based tele-diagnostic interface for breast pathology," in *The 3rd IASTED International Conference on Telehealth*, 2007, p. 130–135.

[8] C.-H. Lee, J. Choi, H. Lee, J. Kim, K. min Lee, and Y. bong Bang, "Exoskeletal master device for dual arm robot teaching," *Mechatronics*, vol. 43, pp. 76–85, 2017.

[9] L. Zhao, T. Yang, P. Yu, and Y. Yang, "An exoskeleton-based master device for dual-arm robot teleoperation," in *2020 Chinese Automation Congress (CAC)*, 2020, pp. 5316–5319.

[10] J. Rebelo, T. Sednaoui, E. B. den Exter, T. Krueger, and A. Schiele, "Bilateral robot teleoperation: A wearable arm exoskeleton featuring an intuitive user interface," *IEEE Robotics Automation Magazine*, vol. 21, no. 4, pp. 62–69, 2014.

[11] M. Mallwitz, N. Will, J. Teiwes, and E. A. Kirchner, "The capio active upper body exoskeleton and its application for teleoperation," in *Proceedings of the 13th Symposium on Advanced Space Technologies in Robotics and Automation. ESA/Estec Symposium on Advanced Space Technologies in Robotics and Automation (ASTRA-2015). ESA*, 2015.

[12] T. Hulin, K. Hertkorn, P. Kremer, S. Schätzle, J. Artigas, M. Sagardia, F. Zacharias, and C. Preusche, "The dlr bimanual haptic device with optimized workspace," in *2011 IEEE International Conference on Robotics and Automation*, 2011, pp. 3441–3442.

[13] J. Chen, D. Hu, W. Sun, X. Tu, and J. He, "A novel telerehabilitation system based on bilateral upper limb exoskeleton robot," in *2019 IEEE International Conference on Real-time Computing and Robotics (RCAR)*, 2019, pp. 391–396.

[14] R. Soltani-Zarrin, A. Zeiaee, A. Eib, R. Langari, N. Robson, and R. Tafreshi, "Tamu cleverarm: A novel exoskeleton for rehabilitation of upper limb impairments," in *2017 International Symposium on Wearable Robotics and Rehabilitation (WeRob)*, 2017, pp. 1–2.

[15] Y. Shen, J. Sun, J. Ma, and J. Rosen, "Admittance control scheme comparison of exo-ul8: A dual-arm exoskeleton robotic system," in *2019 IEEE 16th International Conference on Rehabilitation Robotics (ICORR)*, 2019, pp. 611–617.

[16] E. A. Kirchner, J. C. Albiez, A. Seeland, M. Jordan, and F. Kirchner, "Towards assistive robotics for home rehabilitation." in *Biodevices*, 2013, pp. 168–177.

[17] A. Schiele, "Performance difference of bowden cable relocated and non-relocated master actuators in virtual environment applications," in *2008 IEEE/RSJ International Conference on Intelligent Robots and Systems*, 2008, pp. 3507–3512.

[18] T. Chen, R. Casas, and P. S. Lum, "An elbow exoskeleton for upper limb rehabilitation with series elastic actuator and cable-driven differential," *IEEE Transactions on Robotics*, vol. 35, no. 6, pp. 1464–1474, 2019.

[19] Q. Wu, X. Wang, F. Du, and J. Xu, "Development and control of a bowden-cable actuated exoskeleton for upper-limb rehabilitation," in *2014 IEEE International Symposium on Robotic and Sensors Environments (ROSE) Proceedings*. IEEE, 2014, pp. 7–12.

[20] A. Schiele and G. Hirzinger, "A new generation of ergonomic exoskeletons - the high-performance x-arm-2 for space robotics telepresence," in *2011 IEEE/RSJ International Conference on Intelligent Robots and Systems*, 2011, pp. 2158–2165.

[21] Y. Wang, B. Metcalfe, Y. Zhao, and D. Zhang, "An assistive system for upper limb motion combining functional electrical stimulation and robotic exoskeleton," *IEEE Transactions on Medical Robotics and Bionics*, vol. 2, no. 2, pp. 260–268, 2020.

[22] N. Hogan, "Impedance control: An approach to manipulation: Part i – theory," 1985.

[23] K. Kiguchi and Y. Hayashi, "An emg-based control for an upper-limb power-assist exoskeleton robot," *IEEE Transactions on Systems, Man, and Cybernetics, Part B (Cybernetics)*, vol. 42, no. 4, pp. 1064–1071, 2012.

[24] C. Carignan, J. Tang, S. Roderick, and M. Naylor, "A configuration-space approach to controlling a rehabilitation arm exoskeleton," in *2007 IEEE 10th International Conference on Rehabilitation Robotics*, 2007, pp. 179–187.

[25] F. Porcini, D. Chiaradia, S. Marcheschi, M. Solazzi, and A. Frisoli, "Evaluation of an exoskeleton-based bimanual teleoperation architecture with independently passivated slave devices," in *2020 IEEE International Conference on Robotics and Automation (ICRA)*, 2020, pp. 10 205–10 211.

[26] J. Rebelo, T. Sednaoui, E. B. den Exter, T. Krueger, and A. Schiele, "Bilateral robot teleoperation: A wearable arm exoskeleton featuring an intuitive user interface," *IEEE Robotics Automation Magazine*, vol. 21, no. 4, pp. 62–69, 2014.

[27] J. Lanini, T. Tsuji, P. Wolf, R. Riener, and D. Novak, "Teleoperation of two six-degree-of-freedom arm rehabilitation exoskeletons," in *2015 IEEE International Conference on Rehabilitation Robotics (ICORR)*, 2015, pp. 514–519.

[28] T. Klamt, M. Schwarz, C. Lenz, L. Baccelliere, D. Buongiorno, T. Cichon, A. DiGuardo, D. Droeschel, M. Gabardi, M. Kamedula *et al.*, "Remote mobile manipulation with the centauro robot: Full-body telepresence and autonomous operator assistance," *Journal of Field Robotics*, vol. 37, no. 5, pp. 889–919, 2020.

[29] Y. Ishiguro, T. Makabe, Y. Nagamatsu, Y. Kojio, K. Kojima, F. Sugai, Y. Kakiuchi, K. Okada, and M. Inaba, "Bilateral humanoid teleoperation system using whole-body exoskeleton cockpit tablis," *IEEE Robotics and Automation Letters*, vol. 5, no. 4, pp. 6419–6426, 2020.

[30] J. Lanini, T. Tsuji, P. Wolf, R. Riener, and D. Novak, "Teleoperation of two six-degree-of-freedom arm rehabilitation exoskeletons," in *2015 IEEE International Conference on Rehabilitation Robotics (ICORR)*. IEEE, 2015, pp. 514–519.

[31] J. Rebelo, T. Sednaoui, E. B. Den Exter, T. Krueger, and A. Schiele, "Bilateral robot teleoperation: A wearable arm exoskeleton featuring an intuitive user interface," *IEEE Robotics & Automation Magazine*, vol. 21, no. 4, pp. 62–69, 2014.

[32] D. Buongiorno, D. Chiaradia, S. Marcheschi, M. Solazzi, and A. Frisoli, "Multi-dofs exoskeleton-based bilateral teleoperation with the time-domain passivity approach," *Robotica*, vol. 37, no. 9, pp. 1641–1662, 2019.

[33] H. Lee, J. Kim, and T. Kim, "A robot teaching framework for a redundant dual arm manipulator with teleoperation from exoskeleton motion data," in *2014 IEEE-RAS International Conference on Humanoid Robots*. IEEE, 2014, pp. 1057–1062.

[34] P. Herbin and M. Pajor, "The torque control system of exoskeleton exoarm 7-dof used in bilateral teleoperation system," in *AIP Conference Proceedings*, vol. 2029, no. 1. AIP Publishing LLC, 2018, p. 020020.

[35] H. Sadeghian, L. Villani, M. Keshmiri, and B. Siciliano, "Task-space control of robot manipulators with null-space compliance," *IEEE Transactions on Robotics*, vol. 30, no. 2, pp. 493–506, 2013.

[36] A. Toedtheide, E. Pozo Fortunic, J. Kühn, E. Jensen, and S. Haddadin, "A wearable force-sensitive and body-aware exoprosthesis for a transhumeral prosthesis socket," *IEEE Transactions on Robotics, to be published*, 2023.

[37] S. Haddadin, S. Parusel, L. Johannsmeier, S. Golz, S. Gabl, F. Walch, M. Sabaghian, C. Jähne, L. Hausperger, and S. Haddadin, "The franka emika robot: A reference platform for robotics research and education," *IEEE Robotics & Automation Magazine*, vol. 29, no. 2, pp. 46–64, 2022.

[38] A. De Luca and R. Mattone, "Actuator failure detection and isolation using generalized momenta," in *2003 IEEE International Conference on Robotics and Automation (Cat. No.03CH37422)*, vol. 1, 2003, pp. 634–639 vol.1.

[39] M. A. Gull, S. Bai, and T. Bak, "A review on design of upper limb exoskeletons," *Robotics*, vol. 9, no. 1, p. 16, 2020.